Applied Catalysis B: Environmental 140–141 (2013) 189–198

Contents lists available at SciVerse ScienceDirect

Applied Catalysis B: Environmental

journal homepage: www.elsevier.com/locate/apcatb

Fabrication of wire mesh-supported ZnO photocatalysts protected against photocorrosion

Tan T. Vu, Laura del Río, Teresa Valdés-Solís, Gregorio Marbán *

Instituto Nacional del Carbón (INCAR-CSIC) – c/Francisco Pintado Fe 26, 33011, Oviedo, Spain

ARTICLE INFO

Article history:
Received 4 February 2013
Received in revised form 5 April 2013
Accepted 9 April 2013
Available online 13 April 2013

Keywords:
Methylene blue
Photocatalysis
Photocorrosion
ZnO
Stainless steel wire mesh

ABSTRACT

In this work a catalyst consisting of high surface area ZnO nanoflowers supported on a stainless steel wire mesh was synthesized by hydrothermal growth, and tested for the catalytic photodegradation of methylene blue under UV irradiation. The stability of the photocatalyst was evaluated by assessing the evolution over several reaction stages of catalytic activity and ZnO loss. The initial high activity of this catalyst was followed by a significant decrease after successive reaction cycles due to the dissolution of the ZnO as a consequence of photocorrosion. Impregnation of the catalyst with small amounts of silver enhanced its initial catalytic activity, but failed to produce the photostabilisation of the catalyst that has been reported in the literature. Dip-coating the photocatalyst (either undoped or silver doped) with a diluted polysiloxane solution produced a transparent polysiloxane coating that completely prevented photocorrosion and allowed a stable catalytic activity to be maintained over 8 reaction stages at values higher than those obtained with uncoated catalysts after just 2–3 reactions stages with negligible loss of ZnO.

1. Introduction

Heterogeneous photocatalysts are widely used for the destruction of organic pollutants in wastewaters [1]. For this purpose semiconductor particles, such as TiO_2 and ZnO, have attracted widespread attention [2–4]. TiO_2, as a semiconductor oxide, is a very efficient low-cost photocatalyst that is widely available [5]. Zinc oxide shares many of the properties of TiO_2 [6,7]. Both have similar bandgap energies of around 3.2 eV [6] and it has been found that ZnO nanoparticles may provide a higher quantum yield than TiO_2 nanoparticles [8]. Additionally ZnO has the capacity to absorb a larger fraction of the solar spectrum than TiO_2 [9] and its price is even lower than that of TiO_2 [6]. A major drawback of TiO_2 is the technological limitation associated with the recovery and reutilization of fine titania powders, an important disadvantage that prevents its large-scale implementation in photocatalytic processes. On the other hand, ZnO can be easily fabricated by crystal growth on different supports using low temperature methods [10]. In this way monolithic configurations of the catalyst can be produced and applied under practical conditions.

Unfortunately, the application of ZnO as a photocatalyst is limited due to photocorrosion under UV irradiation in aqueous solutions, which results in a decrease in photocatalytic activity [11–13]. Photocorrosion consists of the partial dissolution of Zn and the collapse of the ZnO structure induced by the action of the UV irradiation. Photocorrosion occurs via the following self-oxidation reactions [14–16]:

$$ZnO + 2\,h^+ + nH_2O \rightarrow Zn(OH)_n^{(2-n)+} + 1/2O_2 + nH^+ \quad (1)$$

$$ZnO + 2\,h^+ \rightarrow Zn^{2+} + 1/2O_2 \quad (2)$$

where h^+ are the positive holes created by the action of UV irradiation. Several research groups have investigated how to reduce ZnO photocorrosion by means of procedures such as depositing silver [17–21], polyaniline monolayers [22], graphitic carbon [23], Nafion films [24], AlSi nanoclays [25] on the surface of the ZnO, via hybridization of ZnO with C_{60} [14] or by depositing ZnO on SiO_2 particles [26].

Although the above modifications help to improve the photocatalytic activity of ZnO some problems still persist. For instance, Bessekhouad et al. have reported that the photocatalytic activity of the doped materials is impaired by thermal instability and by an increase in the number of hole/electron recombination centres [27]. Furthermore, photocorrosion is commonly evaluated by its impact on the photocatalytic activity of the materials, whereas the weight loss of catalysts due to ZnO dissolution is not normally measured. Without this information, other factors such as possible changes in the intrinsic activity of the remaining solid ZnO due to surface reorganization or the photocatalytic activity of colloidal ZnO particles [28] detached from corroded ZnO particles are also overlooked.

* Corresponding author. Tel.: +34 985119090; fax: +34 985297662.
E-mail address: greca@incar.csic.es (G. Marbán).

0926-3373/$ – see front matter © 2013 Elsevier B.V. All rights reserved.
http://dx.doi.org/10.1016/j.apcatb.2013.04.023

In short, when testing these materials it is necessary to evaluate simultaneously the evolution of the Zn loss and catalytic activity over successive reaction cycles.

Dastjerdi et al. have demonstrated a novel technique to stabilize photoactive nanoparticles on a textile surface [29] by using polysiloxane (XPs). They used a self-cleaning and antibacterial cloth coated with Ag/TiO_2 nanoparticles protected by a small amount of XPs. The thin layer of XPs had the effect of isolating the nanoparticles, thus preventing the exchange of electrons between Ag and TiO_2. This exchange causes a red shifted plasmon peak and an impairment of the cloth with an anaesthetic brown colour. With this protection technique the photocatalytic activity of TiO_2 is not negatively affected by the presence of XPs. The present work aims to test this procedure as a method for protecting ZnO nanoparticles against photocorrosion.

In previous works, we tested various procedures for preparing stainless steel wire mesh-supported ZnO catalysts [10]. The catalysts were evaluated for the catalytic photodegradation of methylene blue under ultraviolet irradiation [30]. Some of the tested catalysts showed a higher catalytic activity than that of TiO_2 P25 (Evonik). Unfortunately, even the best catalysts became partly deactivated during the reaction due to ZnO photocorrosion. In this work, a novel procedure [31] has been used to prepare a high surface area ZnO catalyst supported on stainless steel wire mesh. In addition, the catalyst was subjected to silver doping by either photodeposition or equilibrium impregnation in order to study their possible positive effects [18,32] on the activity and stability of the resulting catalyst. Finally, the effect of XPs coating was thoroughly analyzed in order to determine the best conditions for preparing a highly stable catalyst with the best possible catalytic activity for methylene blue decomposition.

2. Experimental

2.1. Catalyst

2.1.1. Materials

All chemical reagents were of analytical grade and were not subjected to additional purification. All of the aqueous solutions were prepared with deionised water. The support was a stainless steel wire mesh [with a 30 μm wire diameter and 40 μm screen opening] provided by CISA. The following reagents were used: zinc acetate dehydrate (Prolabo), silver acetate (99%, Sigma–Aldrich), urea (>99.5%; Fluka), polysiloxane CT208E emulsion supplied by Wacker Finish. The photocatalytic experiments were performed over aqueous solutions of methylene blue monohydrate (>96%; Riedel de Häen).

2.1.2. Synthesis of wire mesh-supported ZnO

The synthesis of wire mesh-supported ZnO was performed on supports consisting of rectangular pieces of wire mesh ($5 \times 3\ cm^2$), previously washed with HNO_3 (4 M) at 60 °C for 4 h and then with isopropyl alcohol in an ultrasonic bath for 10 min.

Mesoporous ZnO nanosheets were synthesized on the surface of the wire mesh by a method that Kakiuchi et al. [31] designed for preparing ZnO on ITO supports. Zinc acetate dehydrate was dissolved together with urea in deionized water. Concentrations of Zn^{2+} and urea in the aqueous solutions were adjusted to 0.05 and 1.0 M, respectively. The pH of the solution was adjusted to 4.88 by using acetic acid. The wire mesh was placed in a Teflon autoclave (100 ml) filled with the growth solution. The autoclave was sealed and hydrothermal ZnO growth proceeded at 80 °C for 23 h in a constant-temperature water bath. The ZnO coated-wire mesh was then taken out of the solution, thoroughly washed with deionised water and vacuum-dried at 60 °C. Finally the sample was calcined at 200 °C for 0.5 h in air.

2.1.3. Silver doped-wire mesh supported-ZnO

To dope the wire mesh-supported ZnO with silver two different methods were employed: equilibrium adsorption impregnation (EAI) and photodeposition (PD). PD allowed Ag nanoparticles to form on the catalyst surface [17,19], whereas EAI yielded Ag_2O particles that were reduced to Ag under reactive conditions by photogenerated electrons [18]. Silver photodeposition was carried out in a similar way to that employed by Xie et al. with powdered ZnO [19]. The wire mesh supported-ZnO was immersed in a 50 mL aqueous silver acetate solution (12.7 ppm Ag) under stirring and subjected to UV-irradiation in the photocatalytic reactor for 1 h [17]. Afterwards, the mesh was rinsed with deionized water and dried at room temperature overnight. The Ag/Zn molar ratio in the prepared sample was Ag/Zn = 0.0032, as measured by Atomic Absorption Spectroscopy.

Equilibrium adsorption impregnation was carried out by immersing the catalyst in a solution of silver acetate (12.7 ppm Ag) and kept under mechanical agitation for several hours. Afterwards, the metal wire mesh was removed from the impregnation solution and immersed in deionized water under agitation to remove any salt that had not been chemisorbed. Finally, the wire mesh was vacuum- dried at 60 °C and calcined in air at 250 °C for 30 min. The Ag/Zn molar ratio in the prepared sample was Ag/Zn = 0.0016, as measured by Atomic Absorption Spectroscopy. This ratio is similar to that considered as optimum in [19].

2.1.4. Preparation of polysiloxane-coated catalysts

Dip-coating with water solutions of polysiloxane (XPs) was applied to both undoped and silver-doped wire mesh-supported ZnO catalysts. A dip-coating device designed and fabricated in our lab was used for this purpose (Fig. 1). This apparatus allows the cycling operation to proceed at a controllable speed following a sequence of dip-coating, air blowing and sample heating. First the substrate ($5 \times 5\ cm^2$) was immersed in the XPs solution (0.3–1.5 wt.%) and then slowly extracted at a speed of $2\ cm\ min^{-1}$. The substrate was then passed through the electrical heating section (preheated at 190 °C) at the same speed in order to cure the XPs layer. Only one dip-coating cycle was applied.

2.2. Characterization

2.2.1. Structural characterization

The morphology of the catalysts was studied by means of a scanning electron microscope (SEM, FEI Quanta FEG 650 model) and a transmission electron microscope (TEM, JEM -2100F model) equipped with a detector to perform electron energy loss spectroscopy (EELS). The X-ray diffraction (XRD) patterns of the catalysts were recorded on a Bruker D8 Advance instrument operating at 40 kV and 40 mA and using Cu Kα radiation (λ = 0.15406 nm). The crystal size values were estimated from the XRD pattern by using Scherrer's equation (d_{XRD}). The instrumental contribution to line broadening was taken into account by using the diffraction pattern of corundum as instrumental standard. Nitrogen adsorption isotherms were performed at −196 °C using a Micromeritics ASAP 2020 volumetric adsorption system. The BET surface area was deduced from an analysis of the isotherms in the relative pressure range of 0.04–0.20. UV–vis diffuse reflectance spectroscopy measurements were carried out using a Shimadzu UV-2460 spectrophotometer equipped with an integrating sphere. The spectra were recorded in the range of 200–700 nm. Pure powdered $BaSO_4$ was used as a reference sample.

Ex situ X-ray photoelectron spectroscopy (XPS) was carried out by means of a Specs spectrometer, using Mg-Kα radiation

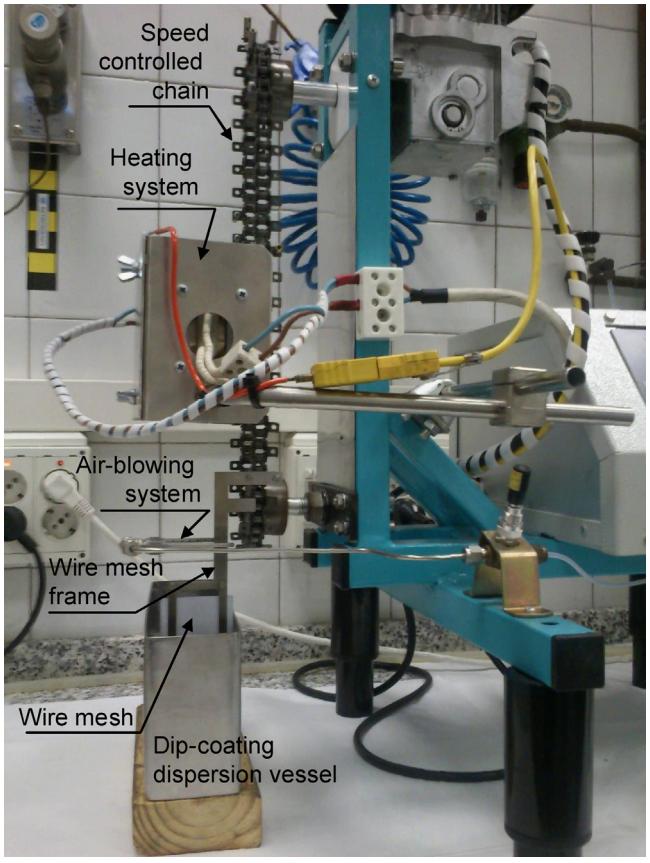

Fig. 1. Dip-coating equipment designed and fabricated in our laboratory.

(1253.6 eV). The binding energies of the spectra recorded were corrected with the binding energy of adventitious carbon in the C1s region (284.6 eV). The backgrounds were subtracted by means of Shirley baselines. The atomic sensitivity factors stored in the CasaXPS database were used for the quantitative analyses.

2.2.2. Photocatalytic tests

The methylene blue photodegradation experiments were carried out with supported catalysts ($1.7 \times 3\,cm^2$ strips weighing ~120 mg) in a 400 mL quartz beaker under the illumination of two ring-type UV 22 W lamps (Luzchem Ring-Illuminator) which predominantly emit radiation at 351 nm. A small clip fixed to the lower end of a vertical rod was used to hold the catalyst strip. The strip and the holder were immersed in 60 mL of a magnetically stirred aqueous solution of methylene blue, with an initial concentration of 10 mg/L. The catalyst was subjected to seven reaction stages (for a total reaction time of 14 h). After each stage the catalyst was extracted from the reaction medium, washed with deionised water, vacuum dried at 60 °C, carefully weighed and re-introduced in the reactor for a new stage with a fresh 10 mg/L methylene blue solution. At each reaction stage the solution was first magnetically stirred for 30 min under darkness to ensure adsorption/desorption equilibrium between the dye and the photocatalyst. Next the reactor was exposed to UV lamps for 120 min. Liquid samples were extracted for measurement at fixed reaction times (0, 15, 30, 50, 80 and 120 min). The visible absorption peaks of the analyzed samples were recorded in the 400–800 nm range by means of a UV–vis spectrometer (Shimadzu UV-2401PC). The true methylene blue concentration was obtained from the visible absorption spectra by means of a recently published deconvolution technique [33] that allows the contribution of reaction intermediates to the spectra to be determined. A photocatalytic analysis was performed using ZnO powder scratched from an undoped wire mesh-supported ZnO catalyst. The powder (10 mg) was suspended in the magnetically stirred liquid for the photocatalytic experiment and the liquid samples for analysis were previously centrifuged to remove the ZnO particles. It was found that the intrinsic catalytic activity of this system was 36% higher than that obtained with the monolithic configuration described above. This difference is ascribed to a higher quantum yield and a better dispersion in the liquid of the suspended powder.

In order to compare the photocatalytic activities of the materials the following factors were taken into account:

(i) the catalyst dosage ($C_{ZnO} = w_{ZnO}/V$, where w_{ZnO} is the weight of ZnO and V is the volume of the liquid) increases slightly due to the regular removal of liquid samples for analysis. Thus, the actual catalyst dosage at any time t can be estimated from the following equation:

$$C_{ZnO} = \frac{w_{ZnO}}{V_0\,(1 - b \times t)} \tag{3}$$

where V_0 is the initial liquid volume and b is a constant that can be evaluated by linear regression;

(ii) the reaction rate can be expressed by the potential equation:

$$-\frac{d\,C_{MB}}{d\,t} = k\,C_{ZnO}\,C_{MB}^{n} \tag{4}$$

where C_{MB} is the methylene blue concentration at a given time t, k is the reaction rate constant ($mg_{MB}{}^{1-n}\,mg_{ZnO}{}^{-1}\,L^{n}\,min^{-1}$) and n is the apparent reaction order. Factor C_{ZnO} is introduced to account for the known dependence of the reaction rate on the catalyst dosage in the absence of screening effects [2,34–36]. Therefore, under chemical control the reaction constant k should be independent of the catalyst dosage.

For $n = 1$, Eq. (4) is coincident with the well-known Langmuir-Hinshelwood equation for diluted solutions [37]. In this case, the resolution of Eq. (4) yields:

$$C_{MB} = C_{MB,0}\exp\left\{-k\,C_{ZnO,0}(1/b)\,\ln\left[1/(1-bt)\right]\right\} \tag{5}$$

whereas for $n \neq 1$:

$$C_{MB} = \{C_{MB,0}^{1-n} - (1-n)\,k\,C_{ZnO,0}(1/b)\,\ln\left[1/(1-b\,t)\right]\}^{1/1-n} \tag{6}$$

where $C_{ZnO,0}$ is the catalyst dosage at $t = 0$. By fitting the concentration values from these equations with the experimental values of C_{MB} at different times, the values of k and n can be obtained. However, the comparison of catalytic activities cannot be performed with the values of k unless the values of n are identical. To overcome this problem, we used the following parameter to evaluate the *intrinsic catalytic activity* of the samples:

$$A_{ZnO} = \frac{1}{t_{0.5}C_{ZnO,0}} \tag{7}$$

where $t_{0.5}$ is the semiconversion time (min). Parameter A_{ZnO} allows the intrinsic activities of the catalysts to be compared at the same initial methylene blue concentration. In principle this parameter is independent of the catalyst dosage [30]. Calculation of $t_{0.5}$ can be performed by re-arranging Eqs. (5) and (6) for $C_{MB} = 0.5 \times C_{MB,0}$. Thus, for $n = 1$:

$$A_{ZnO} = \frac{b}{C_{ZnO,0}\left[1 - \exp\left(-(0.693\,b/k\,C_{ZnO,0})\right]\right.} \tag{8}$$

whereas for $n \neq 1$:

$$A_{ZnO} = \frac{b}{C_{ZnO,0}\left\{1 - \exp\left[-(C_{MB,0}^{1-n}\left(0.5^{1-n} - 1\right)\,b/k\,C_{ZnO,0}(1-n)\right]\right\}} \tag{9}$$

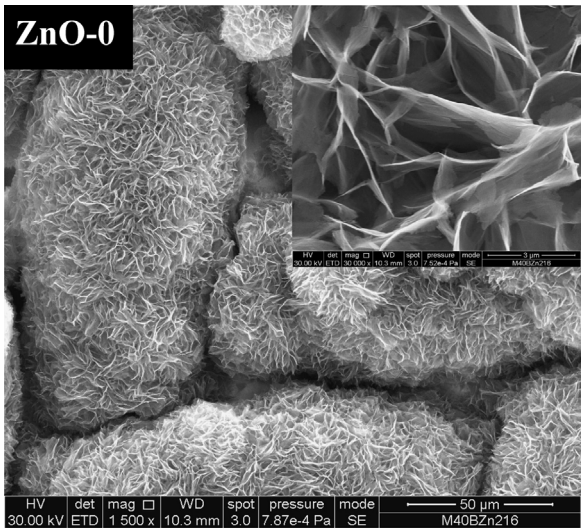

Fig. 2. SEM image of ZnO-0.

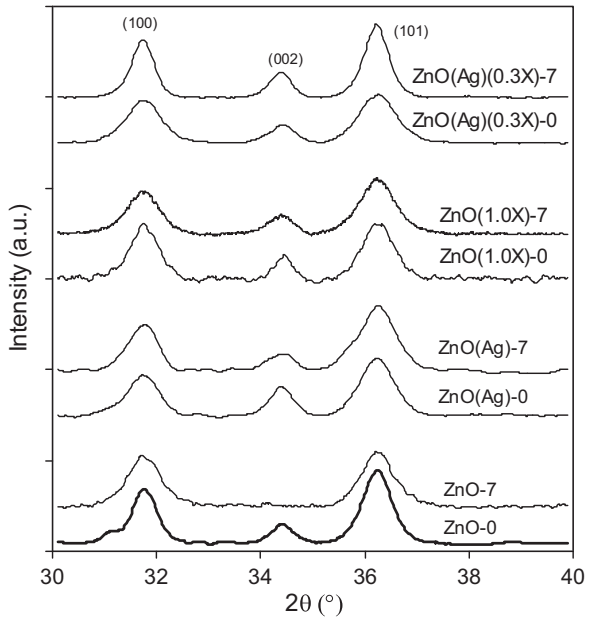

Fig. 3. XRD spectra of different supported catalysts.

This parameter allows the intrinsic activity of different catalysts to be compared on a ZnO mass basis, but in a series of reaction stages performed with the same catalyst it is necessary to consider how the ZnO losses affect the *absolute catalytic activity*. In this situation it is convenient to employ the inverse of the semiconversion time for a fixed initial ZnO dosage (333 mg/L):

$$\frac{1}{t^*_{0.5}} = A_{ZnO} \times 333 \times \frac{C_{ZnO,0}}{C^0_{ZnO,0}} \quad (10)$$

where $C^0_{ZnO,0}$ is the catalyst dosage at the beginning of the first reaction stage (UV time = 0) and $C_{ZnO,0}$ is the catalyst dosage at the beginning of the reaction stage under analysis, in which the catalyst displays the intrinsic activity A_{ZnO}.

2.3. Acronyms

- ZnO-*i*: wire mesh supported-ZnO after having been subjected to *i* reaction stages.
- ZnO(0.3X)-*i*: wire mesh supported-ZnO coated with XPs from a 0.3 wt.% XPs solution after having been subjected to *i* reaction stages.
- ZnO(Ag)-*i*: Ag doped-wire mesh supported-ZnO after having been subjected to *i* reaction stages. If not indicated, Ag doping is performed via Equilibrium Adsorption Impregnation (EAI).
- ZnO(Ag)(0.3X)-*i*: Ag doped-wire mesh supported-ZnO coated with XPs from a 0.3 wt.% XPs solution after having been subjected to *i* reaction stages. If not indicated, Ag doping is performed via Equilibrium Adsorption Impregnation (EAI).

3. Results and discussion

3.1. Unmodified wire mesh supported-ZnO

Fig. 2 shows a SEM image of the ZnO-0 sample (fresh wire mesh supported ZnO). As can be seen ZnO has grown and uniformly covers the microwires of the mesh. The ZnO deposits for all the prepared samples amount to 18.7 ± 5.0 wt.% of the total mass of the coated wire mesh and consist of interconnected nanosheets which are approximately 20–50 nm thick (inset of Fig. 2). This ZnO structure is very open (with voids of 1–3 μm) and has a high BET surface area (75 m^2/g on a ZnO mass basis). The XRD pattern of the ZnO-0 sample is shown in Fig. 3. The indexed peaks correspond to the hexagonal wurtzite structure, according to JCPDS card No. 79-2205. The main characteristic of this pattern is the high (100)/(002) intensity ratio ($I_{100}/I_{002} = 3$), which evidences the exposure of a large proportion of polar surfaces, which is thought to be the key for a high photocatalytic activity [38]. The crystal size of ZnO nanoparticles, as evaluated by the Scherrer equation, is relatively small (13 ± 1 nm).

Fig. 4 shows the results of the MB photodegradation performed with wire mesh supported-ZnO. As can be seen, in the first reaction stage all the MB is degraded in less than one hour, though the catalytic activity is significantly reduced in successive reaction stages. This loss of activity is undoubtedly a consequence of the photocorrosion process, which causes extensive dissolution of the solid ZnO. This is clearly appreciated in Fig. 5, where SEM images of the fresh ZnO-0 sample and of the same sample after having been subjected to 7 reaction stages (ZnO-7) are shown. As can be observed, a significant amount of the initially present ZnO has disappeared from the surface of the wire mesh. The photocorrosion process dissolves a large part of the ZnO, as can be appreciated in Fig. 6. In this figure, the UV time only includes the summation of

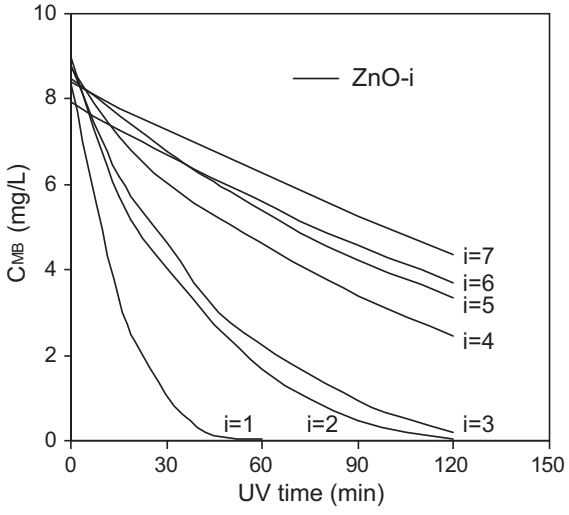

Fig. 4. Methylene blue concentration decay curves for ZnO-*i* (*i* = 1 to 7).

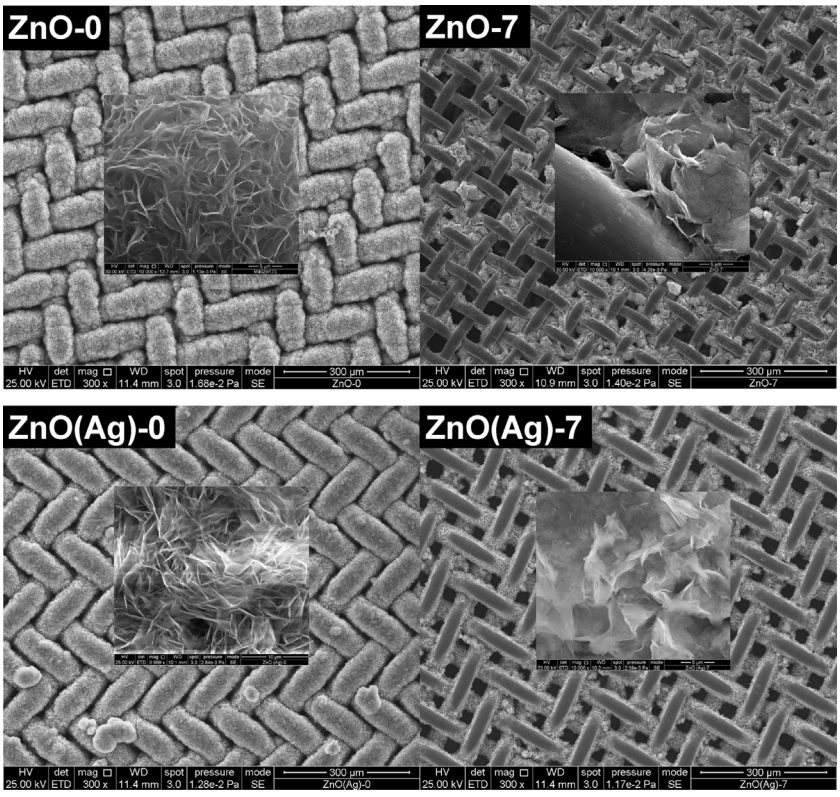

Fig. 5. SEM images of ZnO-0, ZnO-7, ZnO(Ag)-0 and ZnO(Ag)-7.

the reaction times for the successive stages under ultraviolet irradiation. It does not include the adsorption steps under darkness. Each point in the plots stands for one reaction stage (60–120 min). After each stage the catalyst was cleaned with deionized water, dried, weighed and subjected to the next reaction stage. In Fig. 6, the baseline represents the losses of ZnO for a blank experiment in the absence of radiation. These losses are due to manual handling (i.e. fixing the catalyst in the holder after weighing at each stage), which, after seven stages, amounts to less than 3 wt.%. Under reactive conditions, the vast majority of ZnO is lost during the first stage (56.0 wt.%, after the baseline correction, as shown in Fig. 6 and indicated in Table 1), whereas after the seventh stage the lost amount of ZnO has increased to 77.6 wt.%. However, the absolute catalytic activity ($1/t^*_{0.5}$), evaluated by Eq. (10), is much higher in this first stage than in the successive stages (Fig. 6), in which the ZnO losses are not as high as in the first stage. ZnO colloidal particles detached from the corroded ZnO particles probably contribute significantly to the catalytic activity in the first experiment [28]. However, they do not contribute in successive reaction stages, because the MB solution has been renewed. It should also be pointed out that almost 100% of the ZnO detached from the mesh during the photocatalytic test is dispersed or dissolved in the liquid, and only minute traces of ZnO remain as solid particles that can be separated from the liquid by centrifugation. The photocorrosion process causes a clear change in the ZnO crystals. The XRD peak (0 0 2) completely disappears (ZnO-7 pattern in Fig. 3). This implies that the non-polar surfaces are significantly reduced by the corrosion process and, as a result, the intrinsic catalytic activity (A_{ZnO}) of the catalyst should be favoured [38]. However, as can be seen in Table 1, parameter A_{ZnO} for ZnO-1 is twice that of ZnO-7. The reason for this may be the loss of specific surface area as a consequence of photocorrosion. However, the BET analyses only revealed a reduction in specific surface area of from 75 m^2/g (ZnO-0) to 56 m^2/g (ZnO-7), which cannot account for the greater reduction in the A_{ZnO} parameter. The reorganization of the ZnO nanosheets due to photocorrosion probably

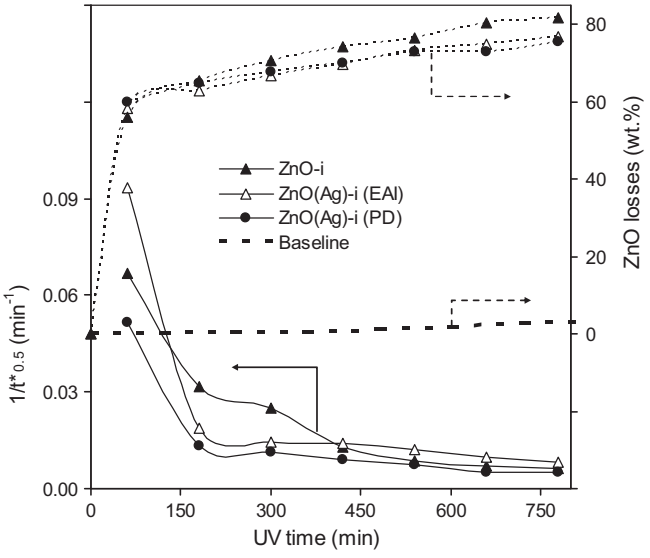

Fig. 6. Variation of absolute activity ($1/t^*_{0.5}$) and ZnO losses during successive reaction stages performed with different supported catalysts. The baseline represents ZnO losses in the absence of UV radiation.

Table 1
Surface atomic relations of Si to Zn obtained by XPS.

Catalyst	Si/Zn	ZnO losses after 7 reaction stages (baseline corrected) (wt.%)
ZnO-0	0	77.6
ZnO(0.3X)-0	0.13	17.1
ZnO(0.6X)-0	1.18	9.7
ZnO(Ag)(0.3X)-0	0.96	8.3

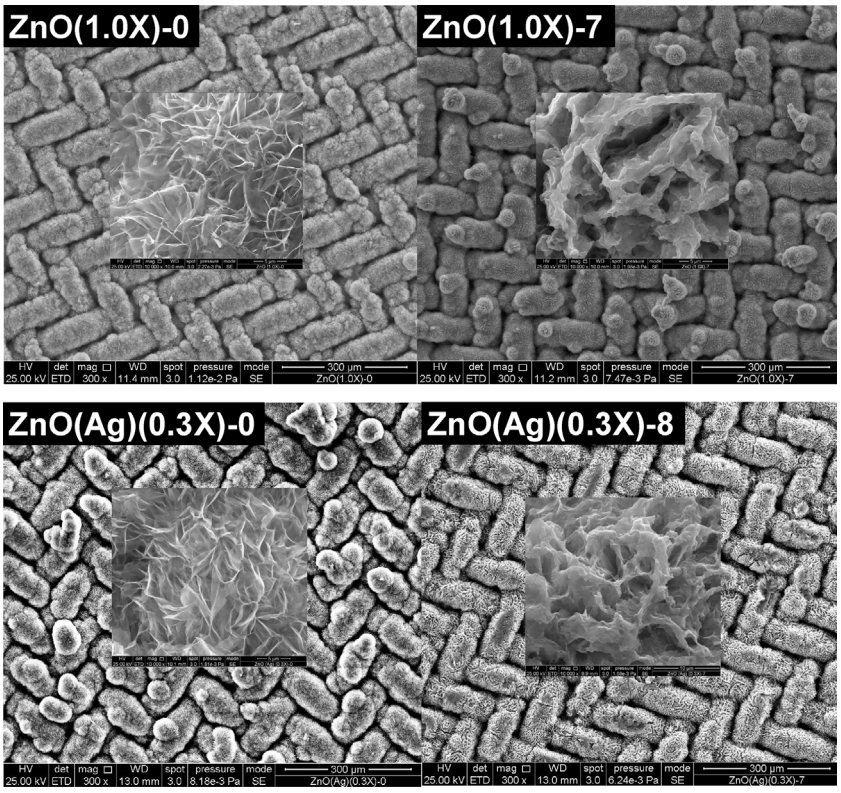

Fig. 7. SEM images of ZnO(1.0X)-0, ZnO(1.0X)-7, ZnO(Ag)(0.3X)-0 and ZnO(Ag)(0.3X)-7.

causes some degree of nanosheet packing. This would hardly affect the value of the specific surface area but it would cause an increase in the extent of the "dark areas" (see insets in Fig. 5 of the SEM images corresponding to ZnO-0 and ZnO-7), and thus would have a negative effect on the quantum yield. In addition, the density of the centres for electron–hole recombination might increase due to the photocorrosion process.

3.2. Ag doped-wire mesh supported-ZnO

Silver doping of the wire mesh supported-ZnO samples should lead to an enhancement of catalytic activity and endow the catalysts with a better stability against photocorrosion [17–20]. Ag nanoparticles on the semiconductor surface act as electron sinks, which provide sites for the accumulation of photogenerated electrons, increase the separation of electrons and holes, and improve photocatalytic activity [17]. Fig. 5 shows the appearance of a silver doped-wire mesh supported-ZnO (ZnO(Ag)-0) prepared by EAI. It can be seen that it is very similar to that of the undoped catalyst (ZnO-0), without any conspicuous accumulations of silver. Contrary to expectations, doping of the catalyst did not produce photostabilisation of the zinc oxide, as is demonstrated by the extensive loss of ZnO detected in the SEM image of ZnO(Ag)-7 (Fig. 5). The ZnO losses for both doped samples (EAI and PD) are very similar to those corresponding to the undoped catalyst (Fig. 6), though their catalytic activities show some differences. Thus, the absolute catalytic activity of the silver doped-catalyst prepared by equilibrium adsorption impregnation shows a clear enhancement with respect to the undoped catalyst in the first reaction stage. However, its activity decreases abruptly in the second reaction stage, remaining more or less constant in successive stages. The silver doped-catalyst prepared by photodeposition is less active than the undoped catalyst, even in the first reaction stage. Again, the photocorrosion process for the silver doped-catalyst reduces the extent of non-polar surfaces, as is reflected by the decrease in the (0 0 2) peak of the XRD spectrum of ZnO(Ag)-7 with respect to that of Zn(Ag)-0 (Fig. 3). This did not cause an increase in the intrinsic catalytic activity of the catalyst (A_{ZnO}), which, as in the case of the undoped catalyst, clearly decreased between the first and the seventh reaction stage (Table 1).

3.3. XPs coated-wire mesh supported-ZnO

In view of the poor photostability achieved by doping the ZnO based-catalysts with silver, we coated the catalysts with solutions of polysiloxane (XPs) in different concentrations, following the idea of Dastjerdi et al. [29]. This procedure reduced the surface area of the catalysts but did not affect the crystal structure of ZnO. Thus, when the catalysts were coated with XPs solution (1.0 wt.%) the specific surface area decreased to 28 m^2/g (on a ZnO mass basis) though the XRD pattern remained unchanged (ZnO(1.0X)-0 in Fig. 3).

Fig. 7 shows a SEM image of ZnO(1.0X)-0. The macroscopic appearance of this catalyst is very similar to that of ZnO-0 (Fig. 5), without any conspicuous accumulations of silicon based-coating. After seven reaction stages the morphology of the ZnO nanosheets has changed to an apparently denser material (see inset in ZnO(1.0X)-7 in Fig. 7) though the zinc oxide seems to remain well adhered to the surface of the wire mesh. In fact, the crystal structure of this "apparently denser" material is practically identical to that of the fresh catalyst, as can be appreciated in the comparison of the XRD patterns for ZnO(1.0X)-0 and ZnO(1.0X)-7 (Fig. 3).

Fig. 8(a–c) shows HRTEM images of ZnO(0.3X)-0. It can be seen that the size of the nanoparticles is rather homogeneous, with an average nanoparticle size of 11.2 ± 2.3 nm, similar to that obtained by XRD (13 ± 1 nm). The lattice spacing of approximately 2.8 Å between adjacent lattice planes (Fig. 8c) corresponds to the (1 0 0) plane of the hexagonal crystalline wurtzite type structure, with space group P63mc, which indicates the exposure of the polar surfaces.

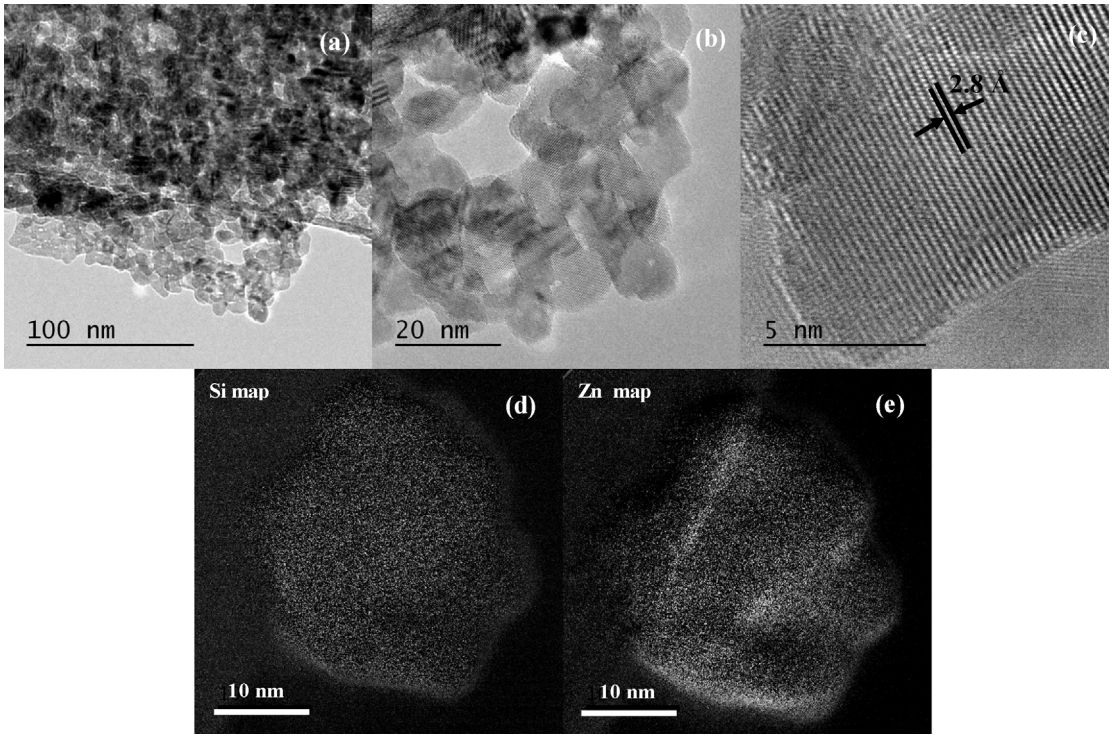

Fig. 8. HRTEM of ZnO(0.3X)-0 (Figs. a–c) and EELS mappings for Si (d) and Zn (e).

No silicon-based particles were visually observed in the images, contrary to what was reported by Siddiquey et al. for silica-coated ZnO particles prepared with TEOS [39], although these authors used a much higher silica content (TEOS/ZnO weight ratios in the range 0.1–0.8). The distribution of silicon and zinc throughout a selected nanoparticle was studied by electron energy loss spectroscopy (EELS) elemental mapping (Fig. 8 d–e). As can be seen, there is a homogeneous distribution of Si throughout the nanoparticle (Fig. 8d). From the combined XRD and HRTEM analyses it can be concluded that XPs is homogeneously distributed over the surface of ZnO as a monolayer and no changes occurred in the ZnO lattice structure after it was dip-coated with XPs.

The surface composition of the catalysts listed in Table 1 was examined by XPS analysis. All the characteristic binding energy peaks corresponding to the expected elements, i.e. Zn, Si, and O, were found, except in the case of the silver-doped catalyst (ZnO(Ag)(0.3X)-0) for which Ag was not visible in the survey scans. The absence of a signal for silver might be explained by the fact that the amount of Ag doped on the surface of ZnO was very small or because silver was shielded by XPs after the dip-coating step.

XPS analyses also show that the amount of surface carbon, which in metallic samples is generally thought to come from the pump oil in the vacuum system of the XPS instrument itself [18], increases linearly with the amount of surface silicon introduced by dip-coating. This must be due to the presence of carbon from alkyl groups of XPs that have not been totally decomposed by the thermal treatment at 190 °C. The C/Si atomic ratio in the original XPs is 8, whereas, after correction for adventitious carbon, the ratio obtained by XPS in the dip-coated samples is 1.4, which indicates that 83% of the original carbon was released during the thermal treatment at 190 °C. Since the cured polysiloxane chains should have a C/Si ratio of 2 [29], the polysiloxane chains covering the ZnO nanoparticles are defective in methyl groups.

The diffuse reflectance absorption spectra of samples ZnO-0 and ZnO(0.6X)-0 are shown in Fig. 9. ZnO(0.6X)-0 exhibited almost the same absorbance edge as the undoped ZnO-0 sample but for a slightly lower absorption in the UV region and a slightly higher adsorption in the visible region, the latter probably due to the presence of carbon in the dip-coated sample. It seems reasonable to conclude therefore that the XPs coating in sample ZnO(0.6X)-0 is almost completely transparent to the incoming radiation.

Fig. 10 shows the evolution curves of the ZnO losses and absolute catalytic activity ($1/t^*_{0.5}$) during consecutive reaction stages corresponding to wire mesh supported-ZnO catalysts coated with different XPs solutions. As can be appreciated, the catalytic activity of the coated catalysts in the first reaction stage is lower than that of the uncoated catalyst, although it remains practically unaltered in successive reaction stages. After 3–4 reaction stages, the activity of the coated catalysts becomes greater than that of ZnO-*i*. The loss of ZnO by the coated catalysts diminishes with the increase in the concentration of XPs in the coating solution, although even in the case of the least concentrated solution the ZnO losses are around 4 times lower than in the case of the uncoated catalysts. In the search for a compromise between catalytic activity and ZnO loss it can be

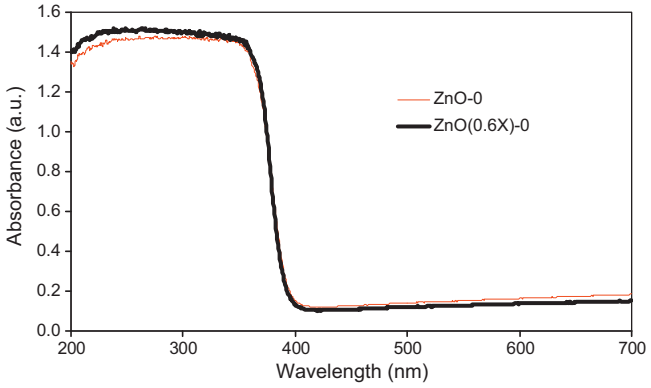

Fig. 9. UV–vis diffuse reflectance spectra corresponding to ZnO-0 and ZnO(0.6X)-0 samples.

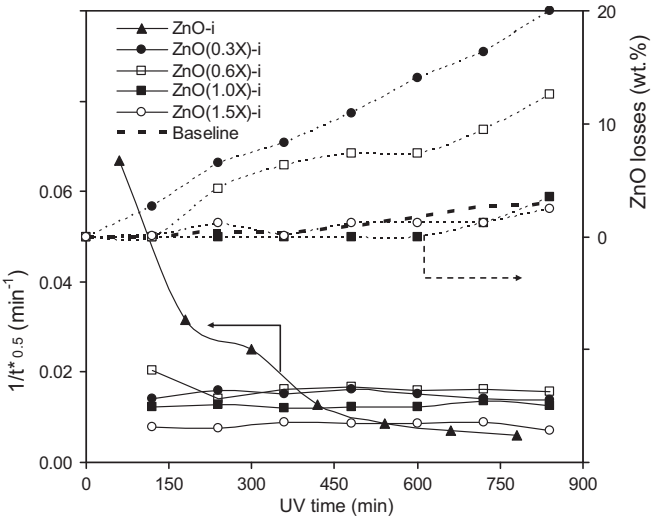

Fig. 10. Variation of absolute activity ($1/t^*_{0.5}$) and ZnO losses during successive reaction stages performed with supported catalysts protected with XPs.

seen that the best catalyst is ZnO(1.0X), because its catalytic activity after seven reaction stages is similar to those of ZnO(0.3X) and ZnO(0.6X) and its loss of ZnO, corrected with respect to the baseline, is zero.

Since the catalytic activity of the silver doped-catalyst (EAI) is higher than that of the undoped catalyst in the first reaction stage (Fig. 6), one would expect coating the silver doped-catalyst to produce a better performing catalyst than ZnO(1.0X). Therefore, we coated two silver doped-catalysts with XPs solutions of different concentrations (0.3 and 1.0 wt.%). The silver-doped catalyst coated with 1.0 wt.% XPs solution did not show any catalytic activity at all. This result can be explained by the data presented in Table 1, which shows the surface atomic relation of Si to Zn obtained by XPS for different samples. Sample ZnO(Ag)(0.3X) contains an amount of silicon that is similar to that of sample ZnO(0.6X) though the concentration of the XPs solution used in the dip-coating stage for ZnO(Ag)(0.3X) was half that used for ZnO(0.6X). It seems that the presence of Ag contributes to the capture of a higher amount of XPs in the dip-coating process. The similar silicon contents in both samples is also the reason for their similar ZnO losses (Table 1), which are undoubtedly dependent on the silicon content. Therefore, the inactive silver-doped catalyst coated with 1.0 wt.% XPs must have a silicon content that is even higher than that of ZnO(1.5X)-0 which, as can be seen in Fig. 10, is already relatively inactive. From the results shown in Table 1 it can be concluded that the ZnO surface becomes quite stable for Si/Zn atomic ratios of around 1.

A tentative mechanism for the photocatalytic reaction on the XPs-coated ZnO particles comprises the photoexcitation of the ZnO particles by the incoming UV radiation through the transparent XPs monolayer, the generation of electron–hole pairs on the ZnO electronic bands, the migration of the generated excitons through the XPs monolayer towards the external surface of the coated particles and the final photodegradation reactions on that surface. A too thick XPs layer ($Si/Zn \gg 1$, as in ZnO(1.5X); Fig. 10) provokes the exciton recombination before reaching the external surface of the XPs coating (and thus the loss of catalytic activity) whereas a too thin layer ($Si/Zn < 1$) is insufficient to protect the ZnO particles from the action of water (photocorrosion reaction (1)).

On the other hand, the ZnO(Ag)(0.3X) catalyst displayed a relatively high catalytic activity which was accompanied by a significant reduction in the loss of ZnO (Table 1). The SEM images of the fresh (ZnO(Ag)(0.3X)-0) and recycled (ZnO(Ag)(0.3X)-7) catalysts (Fig. 7) show almost identical changes to those observed between ZnO(1.0X)-0 and ZnO(1.0X)-7, i.e., although no loss of ZnO can be appreciated, the morphology of the ZnO nanosheets has changed to an apparently more denser material. Again, the XRD pattern of ZnO(Ag)(0.3X)-0 is similar to that of ZnO-0, and has remained unchanged after seven reaction cycles (Fig. 3).

Fig. 11a shows the results of MB photodegradation performed with the ZnO(Ag)(0.3X) catalyst. All the reaction curves are located in a narrow region, indicating that catalytic activity has been maintained over successive reaction stages. The average reaction curve is represented by a dashed line in Fig. 11b and can be compared with the reaction curves produced by the uncoated catalyst. Although coating the catalyst clearly reduces its catalytic activity in the first reaction stage, it produces a better performing material in the following stages. Fig. 12 shows that this catalyst is also superior in performance to ZnO(0.3X) and produces a smaller loss of ZnO (8.3 wt.% after seven reaction stages, corrected with respect to the baseline) although in this respect the best catalyst is still ZnO(1.0X) with no ZnO losses.

Table 2 provides a summary of the catalytic results for the main catalysts subjected to one and seven reaction stages. The high photostability supplied by XPs coating is offset by a loss of activity, which nevertheless is much higher than that obtained with the uncoated catalysts after a few reaction cycles. Part of the activity

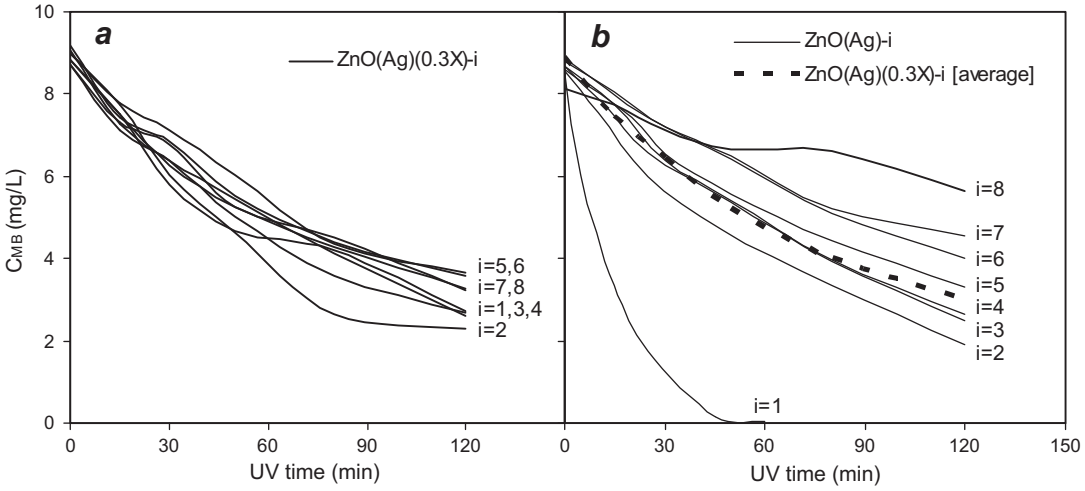

Fig. 11. Methylene blue concentration decay curves for ZnO(Ag)(0.3X)-*i* and ZnO(Ag)-*i* (*i* = 1 to 8).

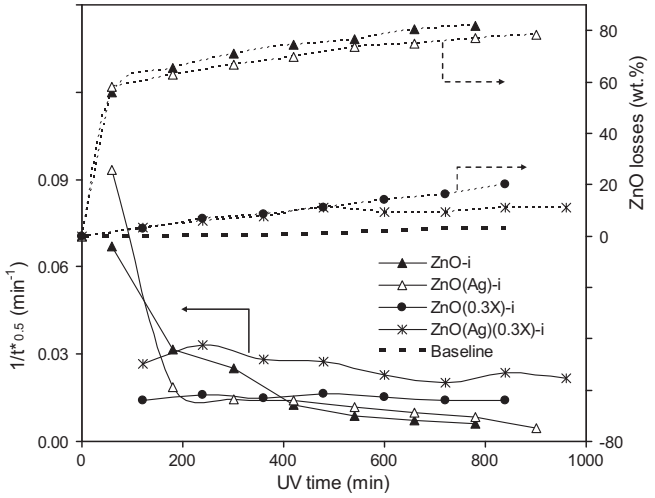

Fig. 12. Variation of absolute activity ($1/t^*_{0.5}$) and ZnO losses during successive reaction stages performed with catalysts consisting of Ag doped-wire mesh supported-ZnO coated with XPs.

Table 2
Summary of catalytic results for catalysts subjected to one and seven reaction stages.

Catalyst	$1/t^*_{0.5} \times 10^2$ (min^{-1})	$A_{ZnO} \times 10^4$ (mg_{ZnO}^{-1} L min^{-1})	ZnO losses (baseline corrected) (wt.%)
ZnO-1	6.69	2.03	56.0
ZnO-7	0.61	0.94	77.6
ZnO(Ag)-1	9.33	2.77	58.2
ZnO(Ag)-7	0.82	0.98	72.0
ZnO(1.0X)-1	1.24	0.37	0.7
ZnO(1.0X)-7	1.26	0.38	−0.4
ZnO(Ag)(0.3X)-1	2.67	0.80	3.5
ZnO(Ag)(0.3X)-7	2.36	0.78	8.3

lost by coating with XPs is due to a decrease in active surface area, though there is also a decrease in intrinsic activity provoked by the XPs coating. Thus, ZnO(1.0X)-1 displays 18% of the intrinsic activity of ZnO-1 ($100 \times 0.37/2.03$), whereas if only the reduction in specific surface area is taken into account, ZnO(1.0X)-1 should retain 37% of the activity of ZnO-1 ($100 \times 28/75$). For the silver doped-catalysts, ZnO(Ag)(0.3X)-1 retains 28% of the intrinsic activity of ZnO(Ag)-1 ($100 \times 0.80/2.77$). The loss of activity associated with the silicon coating might be due to the incorporation of centres of electron–hole recombination. In any case, the values of intrinsic activity (A_{ZnO}) displayed by ZnO(1.0X)-*i* and, especially, ZnO(Ag)(0.3X)-*i* are comparable to, or higher than, those obtained with similar materials, as reported in [30], with the additional feature of having a much greater photostability.

4. Conclusions

In summary, we have synthesized a catalyst consisting of high surface area ZnO nanoflowers supported on stainless steel wire mesh. Doping the catalyst with silver by means of equilibrium impregnation produced an increase in the initial catalytic activity towards methylene blue photodegradation under UV irradiation, but a high degree of photocorrosion was also observed. The photocorrosion process reduced the extent of non-polar surfaces in the ZnO nanosheets although this was not accompanied by the expected increase in intrinsic activity. Dip-coating ZnO and ZnO(Ag) catalysts with diluted polysiloxane solutions produced a homogeneous and transparent XPs coating that provoked the photostabilisation of the catalysts, especially where the surface Si/Zn atomic ratios were over 1. The catalytic activity of the coated catalysts in the first reaction stage was lower than that of the uncoated catalyst, although after a few reaction stages the activities of the coated catalysts were clearly superior to those of the uncoated catalysts. Both the loss of ZnO and catalytic activity during the reaction in the case of the coated catalysts decreased with a greater content of XPs in the coating solution. A compromise between ZnO loss and catalytic activity showed ZnO(1.0X) and ZnO(Ag)(0.3X) to be the optimal catalysts in terms of photocatalytic activity and photostability. The values of intrinsic activity displayed by these catalysts are comparable to, or higher than, those obtained with similar materials, with the additional advantage that they show a much greater photostability.

Acknowledgements

The financial support for this research work provided by the Spanish MEC (CTQ2011-24776) is gratefully acknowledged. Tan T. Vu is grateful to CSIC for the award of a JAE predoc grant.

References

[1] D. Chatterjee, S. Dasgupta, Journal of Photochemistry and Photobiology C: Photochemistry Reviews 6 (2005) 186–205.
[2] M. Ahsan Habib, I.M.I. Ismail, A.J. Mahmood, M. Rafique Ullah, Journal of Saudi Chemical Society 16 (2011) 423–429.
[3] T. Aarthi, P. Narahari, G. Madras, Journal of Hazardous Materials 149 (2007) 725–734.
[4] F. Akbal, Environmental Progress 24 (2005) 317–322.
[5] S.G. Kumar, L.G. Devi, The Journal of Physical Chemistry A 115 (2011) 13211–13241.
[6] W.S. Chiu, P.S. Khiew, M. Cloke, D. Isa, T.K. Tan, S. Radiman, R. bd-Shukor, M.A.A. Hamid, N.M. Huang, H.N. Lim, C.H. Chia, Chemical Engineering Journal 158 (2010) 345–352.
[7] H. Hu, K. Yu, J. Zhu, Z. Zhu, Applied Surface Science 252 (2006) 8410–8413.
[8] C. Lizama, J. Freer, J. Baeza, H.c.D. Mansilla, Catalysis Today 76 (2002) 235–246.
[9] S. Sakthivel, B. Neppolian, M.V. Shankar, B. Arabindoo, M. Palanichamy, V. Murugesan, Solar Energy Materials and Solar Cells 77 (2003) 65–82.
[10] T.T. Vu, L. del Río, T. Valdés-Solís, G. Marbán, Materials Research Bulletin 47 (2012) 1577–1586.
[11] R.T. Sapkal, S.S. Shinde, T.R. Waghmode, S.P. Govindwar, K.Y. Rajpure, C.H. Bhosale, Journal of Photochemistry and Photobiology B: Biology 110 (2012) 15–21.
[12] G. Kenanakis, Z. Giannakoudakis, D. Vernardou, C. Savvakis, N. Katsarakis, Catalysis Today 151 (2010) 34–38.
[13] M. Bitenc, B. Horvat, B. Likozar, G. Dražić, Z.C. Orel, Applied Catalysis B: Environmental 136–137 (2013) 202–209.
[14] H. Fu, T. Xu, S. Zhu, Y. Zhu, Environmental Science and Technology 42 (2008) 8064–8069.
[15] A.L. Rudd, Electrochimica Acta 45 (2000) 1571–1579.
[16] B. Neppolian, H.C. Choi, S. Sakthivel, B. Arabindoo, V. Murugesan, Journal of Hazardous Materials 89 (2002) 303–317.
[17] C. Ren, B. Yang, M. Wu, J. Xu, Z. Fu, Y. Iv, T. Guo, Y. Zhao, C. Zhu, Journal of Hazardous Materials 182 (2010) 123–129.
[18] Z. Yang, P. Zhang, Y. Ding, Y. Jiang, Z. Long, W. Dai, Materials Research Bulletin 46 (2011) 1625–1631.
[19] W. Xie, Y. Li, W. Sun, J. Huang, H. Xie, X. Zhao, Journal of Photochemistry and Photobiology A: Chemistry 216 (2010) 149–155.
[20] C. Tian, Q. Zhang, B. Jiang, G. Tian, H. Fu, Journal of Alloys and Compounds 509 (2011) 6935–6941.
[21] Z. Han, L. Ren, Z. Cui, C. Chen, H. Pan, J. Chen, Applied Catalysis B: Environmental 126 (2012) 298–305.
[22] H. Zhang, R. Zong, Y. Zhu, Journal of Physical Chemistry C 113 (2009) 4605–4611.
[23] L. Zhang, H. Cheng, R. Zong, Y. Zhu, The Journal of Physical Chemistry C 113 (2009) 2368–2374.
[24] J. Wang, P. Liu, S. Wang, W. Han, X. Wang, X. Fu, Journal of Molecular Catalysis A: Chemical 273 (2007) 21–25.
[25] P.S. Suchithra, C.P. Shadiya, A.P. Mohamed, P. Velusamy, S. Ananthakumar, Applied Catalysis B: Environmental 130–131 (2013) 44–53.
[26] G. Corro, U. Pal, N. Tellez, Applied Catalysis B: Environmental 129 (2013) 39–47.
[27] Y. Bessekhouad, D. Robert, J.V. Weber, N. Chaoui, Journal of Photochemistry and Photobiology A: Chemistry 167 (2004) 49–57.
[28] A.L. Stroyuk, V.V. Shvalagin, S.Y. Kuchmii, Journal of Photochemistry and Photobiology A: Chemistry 173 (2005) 185–194.
[29] R. Dastjerdi, M. Montazer, S. Shahsavan, Colloids and Surfaces B: Biointerfaces 81 (2010) 32–41.
[30] T.T. Vu, L. del Río, T. Valdés-Solís, G. Marbán, Journal of Hazardous Materials 246–247 (2013) 126–134.
[31] K. Kakiuchi, E. Hosono, T. Kimura, H. Imai, S. Fujihara, Journal of Sol-Gel Science and Technology 39 (2006) 63–72.
[32] S. Jung, K. Yong, Chemical Communications 47 (2011) 2643–2645.

[33] G. Marbán, T.T. Vu, T. Valdés-Solís, Applied Catalysis A: General 402 (2011) 218–223.
[34] C.A.K. Gouvea, F. Wypych, S.G. Moraes, N. Duran, N. Nagata, P. Peralta-Zamora, Chemosphere 40 (2000) 433–440.
[35] N. Bouanimba, R. Zouaghi, N. Laid, T. Sehili, Desalination 275 (2011) 224–230.
[36] J.M. Herrmann, Journal of Photochemistry and Photobiology A: Chemistry 216 (2010) 85–93.
[37] Y. Zhang, J.C. Crittenden, D.W. Hand, D.L. Perram, Environmental Science and Technology 28 (1994) 435–442.
[38] A. McLaren, T. Valdés-Solís, G. Li, S.C. Tsang, Journal of the American Chemical Society 131 (2009) 12540–12541.
[39] I.A. Siddiquey, T. Furusawa, M. Sato, N. Suzuki, Materials Research Bulletin 43 (2008) 3416–3424.